CSUG/SPE 138154

Analytical Solutions for Mixed CO2-water Injection in Geothermal Reservoirs

Helmut Wahanik, Instituto Nacional de Matemática Pura e Aplicada, Ali Akbar Eftekhari Delft University of Technology, The Netherlands, J. Bruining, SPE, Delft University of Technology, The Netherlands, Dan Marchesin Instituto Nacional de Matemática Pura e Aplicada, Karl Heinz Wolf, Delft University of Technology, The Netherlands

This paper was prepared for presentation at the Canadian Unconventional Resources & International Petroleum Conference held in Calgary, Alberta, Canada, 19–21 October 2010.

Abstract

Concern about global warming is generating interest in reducing the emissions of greenhouse gases such as CO_2. One way of reducing CO_2 emissions is to replace conventional (hydrocarbon fuels) energy sources for heating buildings by geothermal energy. Recently it was suggested to co-inject carbon dioxide with cold water for simultaneous geothermal energy production and subsurface carbon dioxide storage. Our data correspond to a geothermal energy project proposed for heating the buildings of the Technical University of Delft. After injection of the water/CO_2 mixture a complex interaction between physical transport and the phase redistribution of the components, i.e., water and CO_2, occurs. This redistribution is usually described in terms of local thermodynamic equilibrium. There are no published complete analytical solutions for 1-D problems involving complex thermodynamics that include CO_2 and heat effects in the flow. We take into account the heat effects related to the cold fluid injection and related to the dissolution of CO_2.

We give an analytical solution for the model equations for the temperature and for the flow of CO_2, vapor and water after combined injection of a cold carbon dioxide-water mixture in a geothermal reservoir. Due to high pressures and temperatures, CO_2 is in a supercritical state and it is necessary to determine the phase equilibrium for non-ideal gases. We used a modification of the Peng-Robinson equation of state and an activity coefficient based mixing rule for the thermodynamic calculations. A volume shift procedure is applied to obtain an accurate liquid density. The structure of the solution depends strongly on the injection and initial reservoir conditions. The application of the work is in the effective recovery of heat from geothermal reservoirs with simultaneous CO_2 storage. Moreover, the theory provides fundamental understanding of non-isothermal flow of mixtures undergoing mass transfer between phases. The advantage of the analytical model is that it provides a simple methodology to screen injection conditions for optimal geothermal recovery or maximal storage of carbon dioxide.

Introduction

Concern about global warming is generating interest in reducing the emissions of greenhouse gases such as CO_2. There is a large body of literature concerning the injection of carbon dioxide in aquifers. Practical examples are the injection of the separated carbon dioxide produced in the Sleipner gas field (Kongsjorden, Kårstad et al. 1998; Zweigel, Arts et al. 2004) and the Salah field in Algeria (Riddiford, Wright et al. 2004). One way of reducing CO_2 emissions is to replace conventional (hydrocarbon fuels) energy sources for heating buildings with geothermal energy. An important aspect is the transfer rate of carbon dioxide to the water phase, because the storage volume of dissolved carbon dioxide is much lower than gaseous carbon dioxide (R. Farajzadeh 2010; Gmelin's Handbuch). The use of high quality energy to heat buildings has aroused recent interest in geothermal energy, which has low quality but can be used equally well for space heating. In the Netherlands, there is a geothermal gradient of about 30^oC/km leading to a temperature of around 80^oC at a depth of 2000 m. There are numerous papers that describe injection of cold water in geothermal reservoirs and here we only mention the classical paper of Lauwerier (Lauwerier 1955).

Recently, it has been suggested to combine aquifer sequestration of carbon dioxide with production of geothermal energy. The advantage of simultaneous injection can be twofold: first, the coinjected CO_2 may lead to more efficient heat recovery and secondly, the carbon dioxide injected stays sequestered in the reservoir. In this work, we investigate, using a 1-D model, the

concentration and temperature profiles that would occur in the absence of heat intrusion from the surrounding rock. Our data correspond to a geothermal energy project proposed for heating the buildings of the Technical University of Delft (DAP).

There are only a few references that are concerned with injection of CO_2 in geothermal reservoirs. For this Pruess coined the term CO_2-enhanced geothermal systems (EGS) (Pruess, 2006). Moreover, Pruess (Pruess 2008) performed a numerical simulation to evaluate the mass flow and heat extraction rates from enhanced geothermal injection-production systems that are operated using either CO_2 or water as heat transmission fluid. There are strong effects of gravity on the mass flow and heat extraction due to the large contrast of CO_2 density at cold and hot conditions. The tendency for preferential flow of cold, dense CO_2 along the reservoir bottom can lead to premature thermal breakthrough. The problem can be avoided by producing only from a limited depth interval at the top of the reservoir. Pruess finds occasionally greater heat extraction rates for CO_2 compared to water but the dense cold under-riding carbon dioxide can also lead to less efficient heat transfer. Pritchett examines the heat-sweeping effectiveness in a 300 bar fractured reservoir with a low porosity (1%). The initial reservoir temperature is 200°C, which shows that there is no initial steam in the reservoir. The results show, however, that the heat sweeping efficiency of water is better than of CO_2 under these conditions (Pritchett 2009). The advantage as to the storage of CO_2 is not considered in these papers.

After injection of the water/CO_2 mixture a complex interaction between physical transport and the phase redistribution of the components, i.e., water and CO_2, occurs. This paper does not deal with the presence of salt in the water. There are a number of references that deal with a theoretical description of gas injection in aquifers. Zuluaga and Lake consider injection of gases in the near wellbore region where clogging may occur due to evaporation of water (Zuluaga and Lake 2004; Zuluaga and Lake 2005). In (Zuluaga and Lake 2005) the authors formulate the fractional flow model for gas injection in aquifers. We use their model equations in this contribution. Instead of the fractional flow solution we use the wave curve method to determine the Riemann Solution for understanding the wave-pattern evolution corresponding to the injection of a two-phase cold mixture of CO_2/water into porous rock filled with hot water. Riemann solutions exhibit wave fronts found when studying piecewise initial value problems for hyperbolic conservation laws. An example widely used in Petroleum engineering is the solution given by Buckley and Leverett for pure gas or water injection in sandstones filled with oil, as initially described by their famous work (Buckley and Leverett 1942).

An essential feature of the model is transfer between phases. In order to take into account the heat effects related to the cold fluid injection and the dissolution of CO_2, we must understand the fluid-phase equilibrium of the different components in the different phases that appear in the flow. This transfer between phases is usually described in terms of local thermodynamic equilibrium. This requires accurate vapor-liquid equilibrium data. In SPE 93862 (Zuluaga and Lake 2005) an ideal gas approach is used for this purpose. This paper uses thermodynamics of phase equilibria for non-ideal gas behavior. The non-ideal behavior of CO_2-water system has been extensively studied both theoretically and experimentally (Wiebe and Gaddy 1939; King, Mubarak et al. 1992; Bamberger, Sieder et al. 2000; Valtz, Chapoy et al. 2004; Koschel, Coxam et al. 2006). The thermodynamic models used for the prediction of vapor liquid equilibrium have been reviewed in (Orbey and Sandler 1998). Choosing a general model for the calculation of both phase equilibrium and physical properties of a non-ideal mixture would be optimal, but is not yet available. While a selected model may predict the composition of different phases very accurately, it may have weaknesses in the accurate prediction of physical properties, e.g., liquid density. In this work we chose one model and fitted it to the experimental data to achieve accurate prediction of VLE composition and density in each of the phases in a wide range of temperatures and pressures. We give an elaborate description of this model.

During the injection process, a multiphase fluid bank composed of a CO_2-rich supercritical fluid and a H_2O-rich aqueous phase in thermodynamic equilibrium interacts with the reservoir-resident hot water in a complex way. This complex transport process can be described by the evolution of temperature and water/ gas saturation. It is characterized by abrupt changes in the mixture concentrations or temperature, conveniently represented by a combination of shock waves, and rarefaction fans. In summary, Riemann solutions make it possible to understand the mechanisms that occur for injection of cold CO_2/water mixtures in deep hot water reservoirs.

The Model

Our model gives the space-time evolution of the flow resulting from the co-injection of a cold two-phase mixture of carbon dioxide and water into a thin linear horizontal porous core of constant porosity and permeability, initially filled with hot liquid water. We write a system of balance laws for the components of the flow, and for the conservation of energy, taking into account temperature effects. Due to high pressures and temperatures, the CO_2/water mixture is in supercritical state. We consider longitudinal heat conduction, but we disregard transverse conduction with the porous rock. The pressure is assumed to be constant throughout the core; the fluids are considered incompressible. Gravity segregation does not have an important role in the transport process, as the cylindrical core is thin and horizontal. In practice absence of gravity segregation can occur in thin layers with a low vertical to horizontal permeability ratio. Variations of the physical properties of the fluids, e.g., viscosity and composition, can be important due to temperature changes; pressure changes are small along the core and its effect on the physical properties of the fluids is negligible. The 1D Darcy Law for multiphase flow relates the pressure gradient of each phase with its seepage speed

$$u_\alpha = -\frac{k k_{r\alpha}}{\mu_\alpha}\frac{\partial p_\alpha}{\partial x}, \tag{1}$$

where k is the constant absolute permeability of the porous rock and $k_{r\alpha}$ is the relative permeability of phase α. One of the phases is supercritical, denoted by σ, and the other one is an aqueous phase, denoted by a. The realtive permeabilities are functions of their respective saturations, s_σ and s_a. The symbols, μ_α and p_α stand for the viscosity and pressure of phase α.

We write the equations for the conservation of total mass of carbon dioxide (appearing in the supercritical fluid phase, as well as dissolved in the liquid aqueous phase) and water (appearing in the aqueous phase and dissolved in the CO_2-rich supercritical fluid phase) as

$$\frac{\partial}{\partial t}\varphi(\rho_{\sigma c}s_\sigma + \rho_{ac}s_a) + \frac{\partial}{\partial x}(\rho_{\sigma c}u_\sigma + \rho_{ac}u_a) = 0 \tag{2}$$

$$\frac{\partial}{\partial t}\varphi(\rho_{\sigma w}s_\sigma + \rho_{aw}s_a) + \frac{\partial}{\partial x}(\rho_{\sigma w}u_\sigma + \rho_{aw}u_a) = 0\,, \tag{3}$$

where $\rho_{\alpha i}$ denotes the concentration of component i in phase α, (mass [kg] of component i, per unit volume $[m^3]$ of phase α). The different components are carbon dioxide (c) and water (w); φ is the porosity of the porous medium, and assumed to be constant. We include an additional equation for the conservation of energy using the enthalpy density (*i.e.* enthalpy per unit volume) formulation

$$\frac{\partial}{\partial t}\varphi\left(\widehat{H}_r + H_\sigma s_\sigma + H_a s_a\right) + \frac{\partial}{\partial x}(H_\sigma u_\sigma + H_a u_a) = 0\,. \tag{4}$$

The term $\widehat{H}_r$ represents the temperature dependent rock enthalpy density $[J/m^3]$ divided by the porosity φ. The enthalpy density of the supercritical fluid is given approximately by $H_\sigma = \rho_{\sigma c}h_{\sigma C}$. We approximate the enthalpy of the aqueous phase by the enthalpy of H_2O in the liquid phase $H_a \sim \rho_{aw}h_W$ where ρ_{aw} is the partial density of liquid water, taken as the constant 998.2 kg/m^3. Observe that in our analysis we suppose that the contribution to the enthalpy in the corresponding phases comes mainly from their predominant components. The terms $h_{\sigma C}$ and h_W are the temperature dependent specific enthalpies of pure supercritical CO_2 and of pure cooled water given by Span and Wagner, (1996) and by the 1967 IFC Formulation for Industrial Use *resp.*, and interpolated by Reinsch splines (Reinsch,1967) having continuous second derivatives, which suit well the numerical methods used in this paper.

We can perform a practical modification of equations (2), (3) and (4), by performing a straightforward manipulation of expression (1) obtaining

$$u_\sigma = \frac{m_\sigma}{m_\sigma + m_a}u - k\frac{m_\sigma m_a}{m_\sigma + m_a}\frac{\partial p_c}{\partial x}\,, \tag{5}$$

where p_c is the capillary pressure $p_c \stackrel{\text{def}}{=} p_\sigma - p_a$, and $m_\alpha = k_\alpha/\mu_\alpha$ is the mobility of phase α, u is the sum of the Darcy velocities. Observe that $u_a = u - u_\sigma$. Replacing Eq. (5) in the balance laws (2), (3) and (4) we obtain a diffusive term related to the capillary pressure: the effect of this term is to widen the shock, while the convergence of the characteristic lines tries to sharpen the shock. The balance of these effects yields the front width, whose magnitude is negligible compared to the cylinder length. Therefore we may disregard variations of capillary pressure along the core. We may write then

$$u_\alpha = u f_\alpha \tag{6}$$

where f_α is the well known fractional flow function given by $f_\alpha = \frac{m_\alpha}{m_\sigma + m_a}$. In this paper we will use the notation $f \stackrel{\text{def}}{=} f_\sigma$.

Phase equilibria of the CO_2-water system

Phase equilibria of the CO_2-water system play an important role in supercritical fluid extraction and in the CO_2 sequestration processes. Therefore, many experimental data of vapor-liquid and liquid-liquid equilibrium (VLE and LLE) of a CO_2 mixture with other components can be found in the literature. The phase equilibrium plays an important role in the separation of CO_2 from the flue gas. In addition, many efforts have been undertaken to find a comprehensive model that can predict accurately the equilibrium composition and density of the different phases for a wide range of temperatures and pressures. In addition to accuracy, these models should have a relatively fast convergence speed for being practicable in numerical simulations.

Cubic equations of state are reasonably fast in the numerical multicomponent phase equilibrium (flash) calculations. To use an equation of state for the highly nonideal system of CO_2-water, an appropriate mixing rule must be implemented. In this work, we compared different mixing rules for four equations of state and eventually selected the Peng-Robinson-Stryjek-Vera (PRSV) equation of state with the Modified Huron-Vidal second order (MHV2) mixing rule that uses the Non-Random Two-Liquid (NRTL) activity coefficient model. The predicted liquid density by the PRSV equation has been adjusted using the volume shift parameter. The details of the equations and calculation procedure are explained in the next section.

PRSV equation of state with the MHV2 mixing rule

The general form of the PR equation of state (Peng and Robinson 1976) is,

$$P = \frac{RT}{v-b} - \frac{a}{v(v+b)+b(v-b)} \tag{7}$$

where T is the absolute temperature [K], P is the absolute pressure [Pa], v is the specific volume [mol/m3] of the mixture, and R is the universal gas constant with the value of 8.314 Pa.m^3/(mol.K). The effects of the interactions between molecules and the volume of individual molecules are represented by a and b respectively. For each species, the values of a and b are calculated using

$$a_i = 0.457235 \frac{R^2 T_{c_i}^2}{P_{c_i}} \alpha_i(T) \tag{8}$$

and

$$b_i = 0.077796 \frac{RT_{c_i}}{P_{c_i}}, \tag{9}$$

where T_{ci} is the critical temperature [K] and P_{ci} is the critical pressure [Pa] of component i. The parameter $\alpha_i(T)$ is a function of the vapor pressure for each component i and is calculated by the following relation suggested by Stryjek and Vera (Stryjek and Vera 1986)

$$\alpha_i(T) = \left[1 + \kappa_i\left(1 - \sqrt{T_{r_i}}\right)\right]^2 \tag{10}$$

$$\kappa_i = \kappa_{0_i} + \kappa_{1_i}\left(1 + \sqrt{T_{r_i}}\right)\left(0.7 - T_{r_i}\right) \tag{11}$$

$$\kappa_{0_i} = 0.378893 + 1.4897153\omega_i - 0.17131848\omega_i^2 + 0.0196554\omega_i^3, \tag{12}$$

where T_{ri} is the reduced temperature (T/T_{ci}) and ω_i is the acentric factor of component i. Values of κ_{1i} are component specific and are calculated using the vapor pressure data (Orbey and Sandler 1998).

The MHV2 (Dahl and Michelsen 1990) is a modification of Huron and Vidal (HV) mixing rule (Huron and Vidal 1979). For parameter b it uses

$$b = \sum_{i=1}^{N_c} x_i b_i, \tag{13}$$

where N_c denotes the number of components and x_i is the mole fraction of species i in the mixture. To find the parameter a for the mixture, the following quadratic equation must be solved for the variable ε and the larger root must be chosen:

$$q_2\varepsilon^2 + q_1\varepsilon + \left(-q_1\sum_{i=1}^{N} x_i\varepsilon_i - q_2\sum_{i=1}^{N} x_i\varepsilon_i^2 - \frac{g^E}{RT} - \sum_{i=1}^{N} x_i \ln\frac{b}{b_i}\right) = 0. \tag{14}$$

In the above equation, $\varepsilon_i = a_i / b_i RT$ and the value of g^E [J/(mol.K)] is a function of T and x_i. It is calculated using the NRTL activity coefficient model. For the PRSV equation of state the MHV2 model parameters q_1 and q_2 are -0.4347 and -0.003654, respectively (Huang and Sandler 1993). Parameter a can be calculated using the definition $\varepsilon = a/bRT$.

To calculate the fugacity coefficient for each component

$$\ln\hat{\phi}_i = \frac{b_i}{b}(Z-1) - \ln(Z-B) - \frac{1}{2\sqrt{2}}\bar{\varepsilon}_i \ln\frac{Z + \left(1+\sqrt{2}\right)B}{Z + \left(1-\sqrt{2}\right)B} \tag{15}$$

$$\bar{\varepsilon}_i = \frac{q_1\varepsilon_i + q_2\left(\varepsilon^2 + \varepsilon_i^2\right) + \ln\gamma_i + \ln\left(b/b_i\right) + \left(b_i/b\right) - 1}{q_1 + 2q_2\varepsilon}, \tag{16}$$

where $Z=Pv/(RT)$ is the compressibility factor. It is the root of the following dimensionless form of the equation of state:

$$Z^3-(1-B)Z^2+(A-2B-3B^2)Z-B(A-B-B^2)=0, \tag{17}$$

where $A = aP/(RT)^2$ and $B = bP/(RT)$. The smallest positive root of the equation of state represents the liquid phase and the largest one represents the vapor phase compressibility factor.

NRTL activity coefficient model for a binary mixture

The NRTL model (Renon and Prausnitz 1968) is implemented in the estimation of excess Gibbs free energy of the solution and activity coefficient of individual species:

$$\frac{g^E}{RT}=x_1x_2\left(\frac{\tau_{21}G_{21}}{x_1+x_2G_{21}}+\frac{\tau_{12}G_{12}}{x_2+x_1G_{12}}\right) \tag{18}$$

$$\ln\gamma_1=x_2^2\left(\tau_{21}\left(\frac{G_{21}}{x_1+x_2G_{21}}\right)^2+\frac{\tau_{12}G_{12}}{\left(x_2+x_1G_{12}\right)^2}\right) \tag{19}$$

$$\ln\gamma_2=x_1^2\left(\tau_{12}\left(\frac{G_{12}}{x_2+x_1G_{12}}\right)^2+\frac{\tau_{21}G_{21}}{\left(x_1+x_2G_{21}\right)^2}\right), \tag{20}$$

where $\tau_{12} = \Delta G_{12}/(RT)$, $\tau_{21} = \Delta G_{21}/(RT)$, $G_{12} = \exp(-\alpha_{12}\tau_{12})$ and $G_{21} = \exp(-\alpha_{12}\tau_{21})$. For the VLE calculation the value of nonrandomness parameter α_{12} is set to the constant value of 0.3 (Renon and Prausnitz 1969). The other two parameters of the model ΔG_{12} and ΔG_{21} are optimized by fitting the model to the experimental VLE data of CO_2-water system. In this work we assumed that ΔG_{12} and ΔG_{21} are a linear function of the temperature.

Flash calculation, objective function, and optimization

The vapor liquid phase equilibrium (flash) calculation is done using the well-known algorithm of PT-flash that can be found in many references (Walas 1985; Smith, Van Ness et al. 2001). The algorithm calculates the molar fraction of each component in different phases at constant temperature and pressure using the mass balance equations and the following equilibrium condition

$$y_i\Phi_i^V\left(y_i,T,P\right)=x_i\Phi_i^L\left(x_i,T,P\right). \tag{21}$$

Superscripts V and L represent vapor and liquid phases respectively. The mole fraction of each component in the vapor phase is shown by y_i and in the liquid phase by x_i.

The Objective function for the optimization of the NRTL parameters is defined as

$$OF\left(\Delta G_{12}^0,\Delta G_{12}^1,\Delta G_{21}^0,\Delta G_{21}^1\right)=\frac{100}{N}\left(\sum_{i=1}^{N}\frac{\left|x_{CO_2,i}^{\exp}-x_{CO_2,i}^{cal}\right|}{x_{CO_2,i}^{\exp}}+\sum_{i=1}^{N}\frac{\left|y_{water,i}^{\exp}-y_{water,i}^{cal}\right|}{y_{water,i}^{\exp}}\right) \tag{22}$$

where $\Delta G_{12}=\Delta G_{12}^0+\Delta G_{12}^1T$, $\Delta G_{21}=\Delta G_{21}^0+\Delta G_{21}^1T$, N is the number of data points, x_{CO2} is the mole fraction of CO_2 in the liquid phase and y_{water} is the mole fraction of water in the vapor phase. Superscripts '*exp*' and '*cal*' denote the experimental and calculated values, respectively. The experimental VLE data of CO_2-water system of references (Wiebe and Gaddy 1939; King, Mubarak et al. 1992; Bamberger, Sieder et al. 2000; Valtz, Chapoy et al. 2004; Koschel, Coxam et al. 2006) were used in this study. The experimental data are within the temperature range of 278.22 K to 375.10 K and the pressure range of 4.65 bar to 709.28 bar.

The final result is given in Table 1. The model can predict the solubility of gaseous and supercritical CO_2 in water with the average relative deviation of 8.34% represented by the first summation term in Eq. (22) and the solubility of water in gaseous and supercritical CO_2 with 9.67% represented by the second summation term in Eq. (22).

Table 1 Physical parameters of CO_2 and water				
	T_c [K]	P_c [bar]	Ω	κ_1 (PRSV)
CO_2 (1)	304.10	73.7	0.23894	0.04285
Water (2)	647.30	221.2	0.344	-0.06635

Table 2 Fitted parameters of the NRTL model. Subscript 1 is for CO_2 and subscript 2 is for water					
ΔG_{12}^0 (J/mol)	ΔG_{12}^1 (J/mol/K)	ΔG_{21}^0 (J/mol)	ΔG_{21}^1 (J/mol/K)	$\frac{100}{N}\sum_{i=1}^{N}\frac{\left\|x_{CO_2,i}^{\exp}-x_{CO_2,i}^{cal}\right\|}{x_{CO_2,i}^{\exp}}$	$\frac{100}{N}\sum_{i=1}^{N}\frac{\left\|y_{water,i}^{\exp}-y_{water,i}^{cal}\right\|}{y_{water,i}^{\exp}}$
3909.50	18.90	1473.60	16.98	8.34	9.67

To make a correction on the liquid density predicted by the equation of state, the volume shift parameters (Péneloux and Rauzy Richard 1982) were used leading to the following equation

$$v^{real} = v^{cal} + \sum_{i=1}^{N_c} x_i c_i, \tag{23}$$

where c_i [m^3/mol] is the volume shift parameter of component i, v^{cal} [m^3/mol] is the specific volume of the mixture calculated by the equation of state, and v^{real} [m^3/mol] is the experimental specific volume. To calculate the volume shift parameters, we used the data published by Hebach et. al. (Hebach, Oberhof et al. 2004) who reports the density of liquid water in equilibrium with CO_2 in the temperature range of 283.01-333.02 K and the pressure range of 10.9-306.6 bar. As the mole fraction of the aqueous phase is not reported by Hebach et. al., we first calculate the mole fraction using the optimized thermodynamic model and then we use the liquid phase composition to calculate the liquid compressibility factor at constant temperature and pressure. The specific volume of the liquid phase can be calculated as $v^{cal} = ZRT/P$. The objective function for the optimization of volume shift can be defined as

$$OF(c_{CO_2}^0, c_{CO_2}^1, c_{water}^0, c_{water}^1) = \frac{100}{N}\sum_{i=1}^{N}\left(\left|\frac{x_{CO_2}MW_{CO_2} + x_{water}MW_{water}}{v^{cal}} - \rho^{\exp}\right| \Big/ \rho^{\exp}\right), \tag{24}$$

where c_i is a linear function of the temperature $c_i = c_i^0 + c_i^1 T$, N is the number of data points, MW_i is the molecular weight of component i in [kg/mol], x_i is the mole fraction of component i in the aqueous phase, and ρ^{exp} is the experimental value or the density in [kg/m^3]. The optimized volume shift values and the objective function value are given in Table 3.

Table 3 Optimized volume shift values for CO_2 and water for the PRSV-MHV2 equation of state				
$c_{CO_2}^0$ (m^3/mol)	$c_{CO_2}^1$ (m^3/mol/K)	c_{water}^0 (m^3/mol)	c_{water}^1 (m^3/mol/K)	Minimized O.F. value
1.496×10^{-6}	4.706×10^{-9}	-1.072×10^{-7}	-1.012×10^{-8}	0.149

Fig. 1 and Fig. 2 show the experimental VLE data of CO_2-water system and the liquid phase density as a function of temperature at 100 bar.

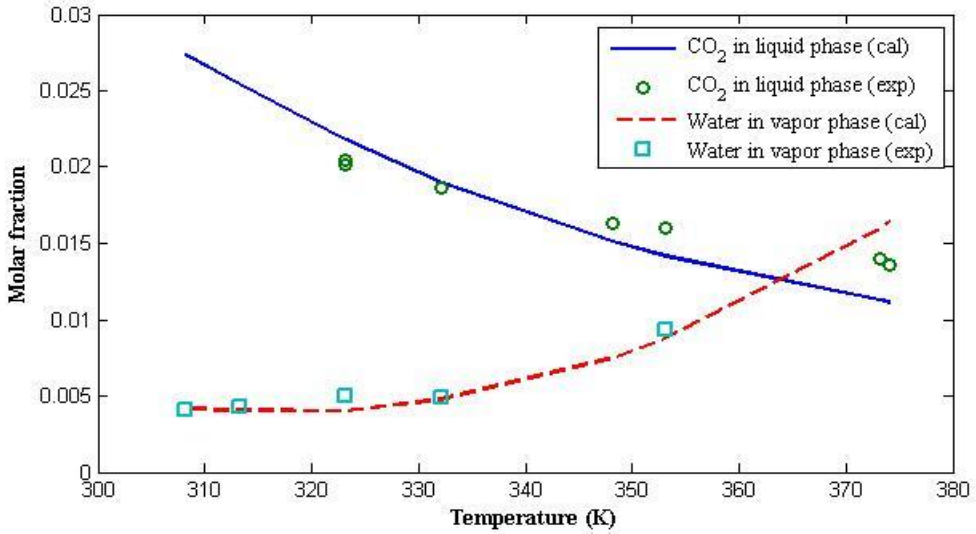

Fig. 1 Equilibrium mole fraction of CO_2 in the liquid phase and H_2O in the vapor phase in different temperatures at 100 bar

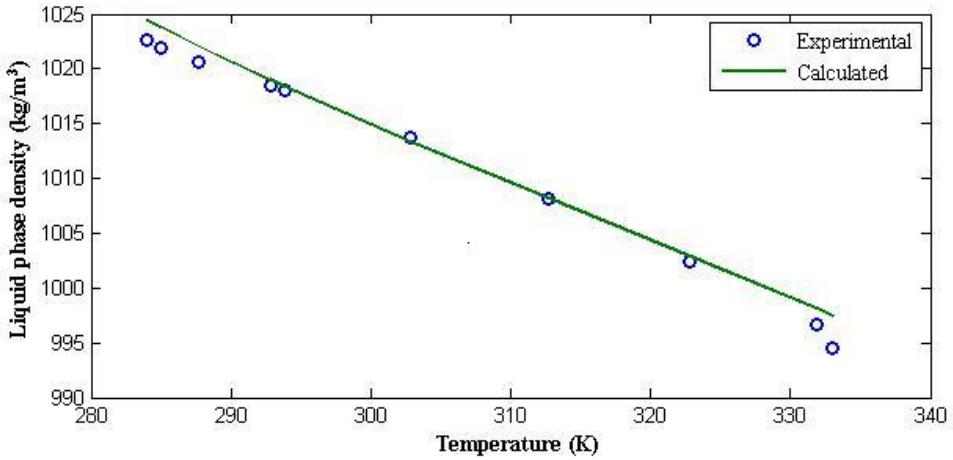

Fig. 2 Density of aqueous phase in the equilibrium mixture of CO_2-water in different temperatures at 100 bar

Mathematical Classification of Wave-Patterns

Our main objective concerns the understanding of wave pattern in fluid transport, consisting of the space-time variations of the different quantities that characterize the flow. Different approaches may provide equivalent insight about the flow evolution. In fact, numerical simulations for systems of conservation laws may provide trustworthy results, even though they usually are computationally time-consuming, quality of the outcome may depend on the appropriate choice of the method to be used (e.g. Finite Volume Hyperbolic for systems of balance, as explained in detail by Leveque (2002)). Their use may fail in furthering the understanding of the core mechanisms in the system of partial differential equations corresponding to the physical model, as well as the classification of the different possible outcomes depending on the inputs of the simulator. Fundamental improvements may be carried out for understanding the physical processes at the pore and reservoir scale through upscaling, as treated in many interesting examples; for instance see Salimi et. al. (2009). In a complementary approach, a mathematical analysis of the structure of the hyperbolic system of conservation laws corresponding to the quantities transported by the flow can provide a bifurcation diagram for the injection problem: inputs for the injection values belonging to the same *region* in the state space exhibit the same flow evolution pattern. Such analytic solution of the injection problem can be obtained by the wave-curve method, summarized in part by Azevedo et. al. (2009). A comprehensive study of this method can be found in Isaacson et. al. (1992). These inputs are the values of the *Riemann-Goursat problem*, written as

$$U(x=0,t)=U_L \quad and \quad U(x,t=0)=U_R \tag{25}$$

where $U(x=0,t)$ are the (injection) boundary values of the unknown quantities, and $U(x,t=0)$ are the known initial conditions of the reservoir. We want to predict the flow evolution, *i.e.* $U(x,t>0)$. In this paper we present the wave sequence found through detailed analysis of the bifurcation diagrams, corresponding to the process of CO_2-EGS, *i.e.* the injection of a cold two-phase mixed CO_2/water mixture into porous rock containing hot water. In the analysis that follows we show how this wave-

pattern classification is carried out by studying the different types of waves that can appear in the flow, and by finding important bifurcation loci where the solutions may change type in state space.

Waves in the Thermodynamic Configurations

As explained above we will concentrate our efforts in an injection problem where the injected fluid is a cold two-phase CO_2/water mixture and the fluid found initially in the reservoir is hot liquid pure water. In this case, we say that the injected fluid is in the *tp* (*t*wo-*p*hase) configuration: a mixture of two phases in thermodynamic equilibrium, one of liquid water with dissolved CO_2, and the other one a CO_2-rich supercritical fluid phase with dissolved H_2O. The fluid found initially in the reservoir, *i.e.* pure hot liquid water, is in the *spa (*single *p*hase *a*queous*)* configuration: a liquid phase composed of liquid water with dissolved CO_2. We assume ideal mixing throughout the flow. We assume that both the *tp* and *spa* configurations are in local thermodynamic equilibrium, therefore Gibbs phase rule $f = c - p + 2$ is satisfied, where f represents Gibbs number of degrees of freedom, and c and p are the number of chemical species and phases, respectively; the number 2 accounts for the temperature and pressure. In the *tp* configuration the pressure is fixed, $c = 2$, and $p = 2$, therefore we obtain f = 1. Therefore, in this configuration the component distribution along the phases is given by the system temperature. We use the complex thermodynamic calculations described before for finding this component distribution accurately for a uniform grid of temperatures, and interpolate the results using smoothing splines (Reinsch, 1967). In particular, we find the partial densities $\rho_{\alpha i}$, where $\alpha = \sigma, a$ and $i = c, w$, as functions of temperature.

We conclude that the balance laws (2), (3) and (4) are expressed in terms of s_σ, T, and u, in the *tp* configuration. We write $U = (V, u)$ where $V = (s_\sigma, T)$. Following this notation, and taking into account the modification (6), the balance laws (2), (3) and (4) can be written as a system of the form,

$$\frac{\partial}{\partial t} G(V) + \frac{\partial}{\partial x} uF(V) = 0 \tag{26}$$

Assuming that are G and F are differentiable functions in space and time, we may write Eq. (26) as

$$B \frac{\partial}{\partial t}\begin{pmatrix} S \\ T \\ u \end{pmatrix} + A \frac{\partial}{\partial x}\begin{pmatrix} S \\ T \\ u \end{pmatrix} = 0 \tag{27}$$

where the letter s stands for s_σ. B and A are the Jacobians of the accumulation term G and the of flux term uF.

We look for self-similar solutions of the Riemann problem for the system of PDE's (27), i.e., solutions that satisfy $U(x,t) = U(x/t)$. Therefore we want to analyze (27) under the change of variables $\tau = x/t$. Applying the chain rule in (27) we obtain

$$(A - \tau B)\frac{dU}{d\tau} = 0 \tag{28}$$

We conclude that a special type of solutions of (27) can be found by looking for solutions of the generalized eigenvalue-eigenvector problem

$$(A - \ l(U)B)r(U) = 0 \tag{29}$$

where

$$U = U(\tau) \tag{30}$$

$$\frac{dU}{d\tau} = r(U) \tag{31}$$

We also imply that the parametrization of $U(\tau)$ satisfies

$$l\big(U(x/t)\big) = x/t. \tag{32}$$

Solutions for the problem stated by (29), (30), (31) and (32) are called *rarefaction (fan) waves*. In the particular case we are studying, due to the linear form in u appearing in the system (3.1.1), two families of eigenvalues and eigenvectors arise

$$l_s = \frac{u}{\varphi}\frac{\partial f}{\partial s} \quad , \qquad r_s = (1,0,0)^T \tag{33}$$

and

$$l_e = \frac{u}{\varphi}\frac{f-f_e}{s-s_e} \, , \qquad r_e = (g_1, g_2, ug_3) \tag{34}$$

where f_e and s_e are functions of temperature , and g_1, g_2 and g_3 are functions of s and T. The expressions f_e and s_e are functions of temperature and have been found after detailed study of the zeros of the directional derivative of l_e along the e-family, i.e., $\nabla l_e(U_e(\tau)) \cdot r_e(U_e(\tau))$, where U_e stands for an e-rarefaction fan.

We see immediately that the s-family (33) (s stands for saturation) corresponds to the Buckley-Leverett characteristic speed. Rarefaction fans for this family are straight lines in the s,T plane, See (33b). Observe also that the eigenvalue l_e in (34a) has the form of a secant to the graph of the Buckley-Leverett fractional flow function.

Condition (32) implies that we can connect points in the (s,T,u)-space using rarefaction fans whenever the eigenvalue increases along the integral curve. Therefore we are interested in studying inflection locus for both families (33) and (34). This locus is a rarefaction fan "stopping" site. In our example, in order to find rarefaction fans, we can restrict to looking for integral curves in the variables s and T, and for inflection locus for both characteristic families. In fact, from the expression of the third component of the eigenvector r_e we see that the total Darcy speed u can be found from the integral curve projected in the variables s and T.

The inflection locus for the Buckley-Leverett family (33) can be found by looking for zeros of $\partial^2 f/\partial s^2$ in the s,T plane. We denote this locus by I_s.

The coincidence locus of e-family (34) (e stands for *evaporation*), denoted by $C_{s,e}$ (i.e., where $l_e = l_s$) is contained in its inflection locus, denoted by I_e. The general theory for bifurcation loci for this kind of multi-component multiphase transport problems was studied by Lambert et. al. (2009). It is easy to show that $\partial l_e/\partial s$=0, and r_e is parallel to r_s on the coincidence curve $C_{s,e}$.

In Fig. 3 we can see the inflection loci for both families. Integral curves were found by integrating numerically the system of ODE's (using a coherent choice of the eigenvector r_e) corresponding to the *tp* configuration using the thermodynamic data obtained above. Above the upper branch and below the lower branch of the coincidence curve C_e , the Buckley-Leverett characteristic speed is slower than the evaporation speed: when localized in one of this regions, when connecting the different waves for finding the solution to the Riemann problem, we should construct the wave-curve corresponding to the solution of the Riemann problem starting with a slow family, exhausting slow-wave pieces and continue the process with a fast family. Therefore when the injection value is in one of these regions, we must start the wave-curve using a Buckley-Leverett wave.

In Fig. 3 we also see the rarefaction curves in the directions of increasing speed. We detail also the orientation of the vector field r_e chosen particularly in this case.

Another kind of self-similar solutions are *shock waves*. Such waves are discontinuities in the solution $U(x,t)$ that satisfy the *Rankine-Hugoniot* condition. The *RH* condition for systems of the type (26) can be expressed as

$$v[G] = u^+F^+ - u^-F^- \tag{35}$$

where $[G] \stackrel{\text{def}}{=} G^+ - G^-$ is the difference between the limit values on the right and left of the discontinuity, and v is the speed of the discontinuity. For this type of systems, we define the *Rankine-Hugoniot Locus* of a given starting value $U^- = (V^-, u^-)$. It is the set of points of the form $U^+ = (V^+, u^+)$ that satisfy relation (35) together with the starting point. It is found by looking for the values of V^+ that satisfy the *RH* condition. It turns out that v and u^+ can be found in terms of the remaining variables. In fact, Eq. (35) can be written as a system of the form:

$$\begin{bmatrix} [G_1] & -F_1^+ & F_1^- \\ [G_2] & -F_2^+ & F_2^- \\ [G_3] & -F_3^+ & F_3^- \end{bmatrix} \begin{bmatrix} v \\ u^+ \\ u^- \end{bmatrix} = 0 \tag{36}$$

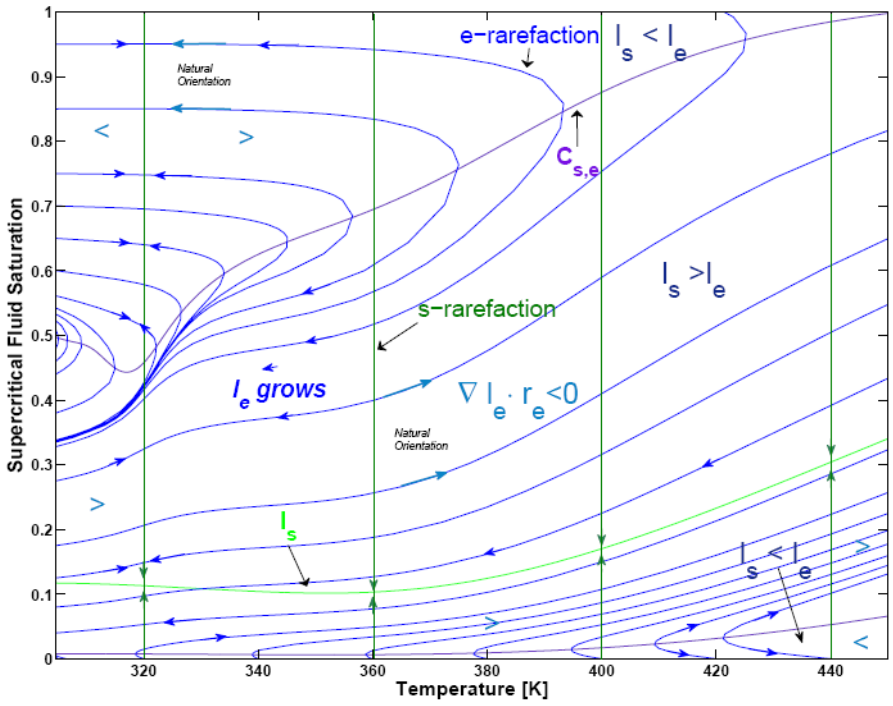

Fig. 3 Rarefactions and inflection loci for the *s* and *e* families.

In fact, the total Darcy speed scales along the shocks (Lambert et. al. 2009); after finding the RH Locus in the variables V passing through the point (V^-, u^-) we will be able to find v and u^+ by solving the linear system (36).

Under certain regularity assumptions, the RH Locus for systems of the type (26) is given by two curves, intersecting at the starting point U^- each tangent to the rarefaction curves and possibly presenting auto-intersections. These two curves belong to different families (slow and fast). Each point U^+ in the RH Locus represents a shock wave between the states $U^-$and U^+ with speed $v = v(U^-, U^+)$. Unfortunately, not all the points belonging to the RH Locus represent physically admissible solutions for the Riemann problem. We must use various admissibility criteria in order to choose the physically correct shocks. For instance in this work we use Lax Shock Admissibility Criteria and Liu E-condition (for a comprehensive study of shock admissibility see Dafermos, 1999). In order to establish the admissible subsets of the RH Locus, we must understand how the characteristics speeds interact on the left and right of the shock. For this reason we compare the shock speed with the slow and fast characteristic speeds on both sides of the shock wave. For instance, in Fig 4 we observe two examples of RH Locus, for different random points in the *tp* configuration. The left state is marked by a × sign, and the different subsets of the RH Locus have been classified according to the shock type: e.g. classical (Slow and Fast Lax) shocks are represented in blue and red. For example, the left-hand slow and fast characteristic speeds collide with the shock (i.e. they are faster than the shock), the slow right-hand characteristic line collides (i.e. it is slower than the shock) and the fast right-hand characteristic speed is faster than the Slow Lax Shock. The comparisons are represented by the + and – sign in Fig. 4.

Contact Discontinuities are particular degenerate shocks; they are abrupt changes in $U(x,t)$ that travel with characteristic speed. They are represented in the space of variables (s, T, u) by integral curves of the system (30), (31) where the eigenvalue l remains constant, i.e. where

$$\nabla l(U) \cdot r(U) = 0 \tag{37}$$

Moreover, these discontinuities satisfy the *RH* Condition. In our case, inside of the *tp* configuration we do not observe this kind of waves. They exist in single phase conditions, e.g., in the single phase aqueous configuration.

As the pressure is fixed in the *spa* configuration, $c = 2$ and $p = 1$, the Gibbs phase rule gives $f = 2$: the degrees of freedom are the composition of H_2O in the aqueous phase ϑ_{aw}, and the temperature T. The variable ϑ_{aw} is defined as $\vartheta_{aw} = \rho_{aw}/\rho_W$, where ρ_{ac} is the density of H_2O in the aqueous phase. The composition of CO_2 in the aqueous phase, is defined as $\vartheta_{ac} = \rho_{ac}/\rho_{aC}$ where ρ_{ac} is the density of CO_2 in the aqueous phase, and ρ_{aC} denotes the density of pure CO_2 in the aqueous phase. The latter is an artificially introduced quantity, and it accounts for the volume increase of carbonated water when found in the *tp* configuration.

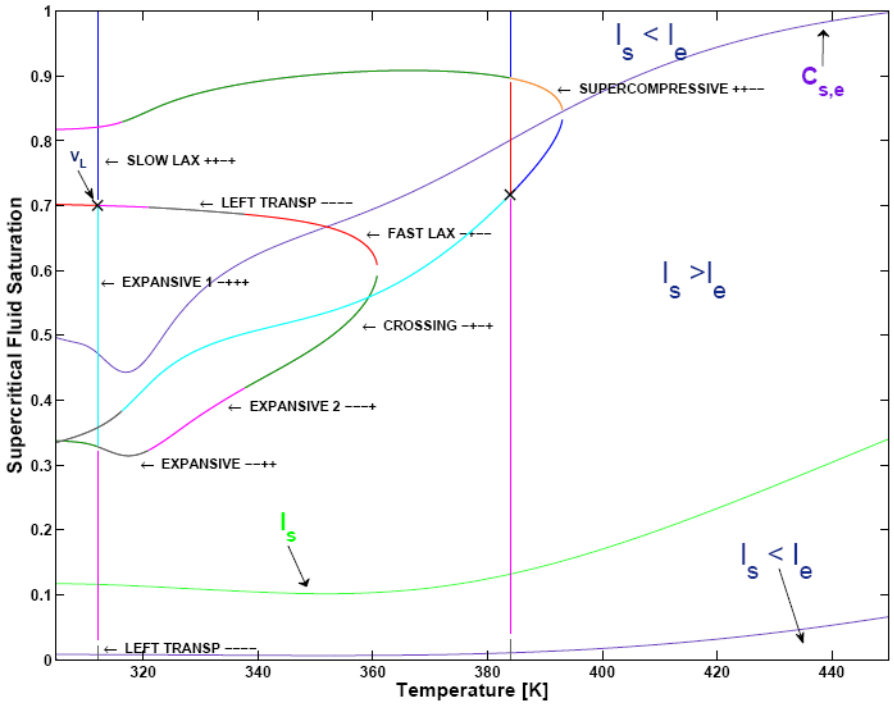

Fig. 4 Example: Injection problem and *RH Locus*.

Observe that ρ_{ac} is a function of temperature. It is found using the ideal mixing rule $\vartheta_{aw}+\vartheta_{ac}=1$ and the data from thermodynamic equilibrium. In the *spa* configuration the value of ϑ_{aw} satisfies the inequality,

$$\vartheta_{aw}^{tp} \leq \vartheta_{aw} \leq 1 \tag{38}$$

where ϑ_{aw}^{tp} corresponds to the composition of H_2O in the aqueous in the *tp* configuration. In fact, the liquid phase becomes carbon saturated at the composition ϑ_{ac}^{tp}. Inequality (38) is a boundary of the *spa* configuration.

We conclude that the balance laws (2), (3) and (4) are expressed in terms of ϑ_{aw}, T, and u, in the *spa* configuration. We write $U = (V, u)$ where $V = (\vartheta_{aw}, T)$ (observe that in this configuration $s_\sigma = 0$). As in the *tp* configuration, in the *spa* configuration the balance laws (2), (3) and (4) can be written as a system of the form (26). It is important to highlight that the form of the accumulation term G and the flux term uF is different in the *tp* and *spa* configuration.

As in the *tp* configuration, due to the linear form in u appearing in the system (26), two families of eigenvalues and eigenvectors arise in the *spa* configuration

$$l_\vartheta = \frac{u}{\varphi}, \qquad r_\vartheta = (1,0,0)^T \tag{39}$$

and

$$l_T = \frac{u}{\varphi}\frac{C_W \vartheta_{aw}}{C_W \vartheta_{aw} + \hat{C}_r}, \quad r_T = (h_1, h_2, uh_3) \tag{40}$$

where

$$C_W = \frac{\partial}{\partial T} H_W, \qquad H_W = \rho_W h_W \tag{41}$$

and h_i , $i = 1,2,3$ are functions of H_2O composition and temperature. In this work we use the approximation $C_W \sim 4.22 \times 10^6 [kJ/m^3 K]$. In this case both families of eigenvalues and eigenvectors satisfy the equality $\nabla l \cdot r = 0$ everywhere; therefore the integral curves in this region parametrize contact waves. As the system is strictly hyperbolic in the ϑ_{aw} and T coordinates, from Lax theory for systems of the type (26) (See Lambert et. al., 2009), the two branches of the RH Locus coincide with the

integral curves that parametrize contact discontinuity waves. From (39.a) and (40.a) we see that T-contacts are slower than ϑ-contacts. When building Riemann solutions containing contact discontinuities we use Liu E-condition as an admissibility criterion. Therefore, we must start the construction with a slow T-contact wave and follow by a fast ϑ-contact wave. In Fig. 5 we show the *spa* configuration together with the *tp* boundary ϑ_{aw}^{tp} and both families of contacts. We also show the *tp* boundary and the initial reservoir state for the Riemann problem treated in the section that follows.

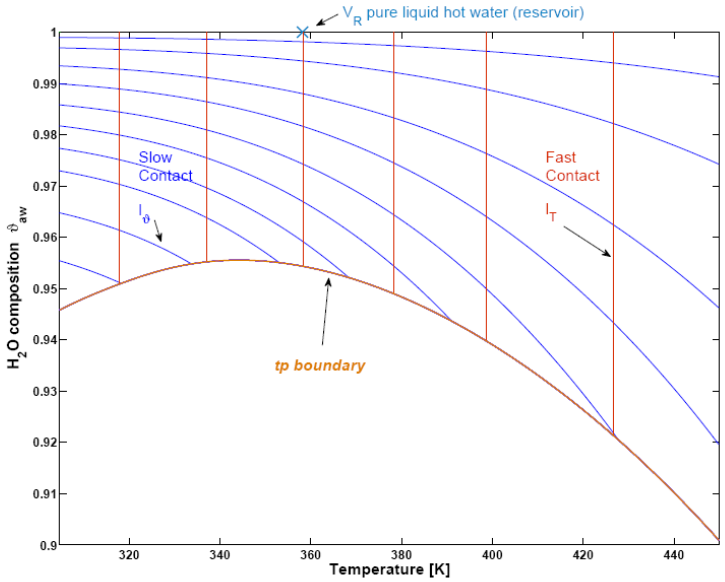

Fig. 5 Waves in the single phase aqueous configuration

The Riemann Solution for a CO_2-enhanced geothermal system

In this section we show the Riemann solution for an specific injection scenario: we inject a two-phase CO_2/water mixture with 50 % weight of carbon dioxide at a temperature of 308.15 [K] with injection rate 4.22×10^{-6} [$m^3/m^2 \cdot s$], in porous rock with pure liquid hot water at 358 [K]. The overall pressure constant value is 100 [bar]. In order to build the wave-curve we must carefully study the compatibility between the speed of the rarefaction fans, shocks waves and contact discontinuities (always starting with slow waves followed by faster waves) and determine the admissibility of the shock waves to be considered.

In compositional flows in porous media modeled by hyperbolic systems of conservation laws, different regions of thermodynamic equilibrium are typically separated by shock waves (see Lambert et. al. 2009). We calculate these shock waves for the particular example of CO_2-EGS treated here, between the *tp* configuration and the *spa* configuration, using the RH condition. We find the RH Locus *between regions* by solving the linear system (36) (using the appropriate accumulation terms G_α and F_α, $\alpha = tp, a$, at both sides of the shock): we fix a right state (V_a^+, u_a^+) in the *spa* configuration and find the left states V_{tp}^- together with the shock speed v and u_{tp}^-. These discontinuities between the *tp* and *spa* configurations will be called *tp-a* shocks. Note that both regions have a boundary in common given by the curve (parametrized by T) ($s_\sigma = 0$, T , $\vartheta_{aw}^{tp}(T)$), over the temperature interval $T_{UCEP} \leq T \leq T_{dew}$, where T_{UCEP} is the upper critical temperature (*UCEP*, 304.63 [K] and 74.11 [bar], Wendland et. al., 1999) and $T_{dew} \sim 551$ [K] is the dew point of the CO_2/water mixture at constant pressure found with a standard dew point calculation (Walas, 1985).

After a mass balance calculation we find that the injection value for the supercritical fluid saturation is $s_\sigma = 0.5713$. The *left* state (injection) $(x = 0,\ t > 0)$ is denoted by V_L, see Fig. 6 and Fig. 7. The *right* state (reservoir) $(x > 0)$ is denoted by V_R, see Fig. 5. In Figs. 6-7 we show the wave curves used in the construction of the Riemann solution.

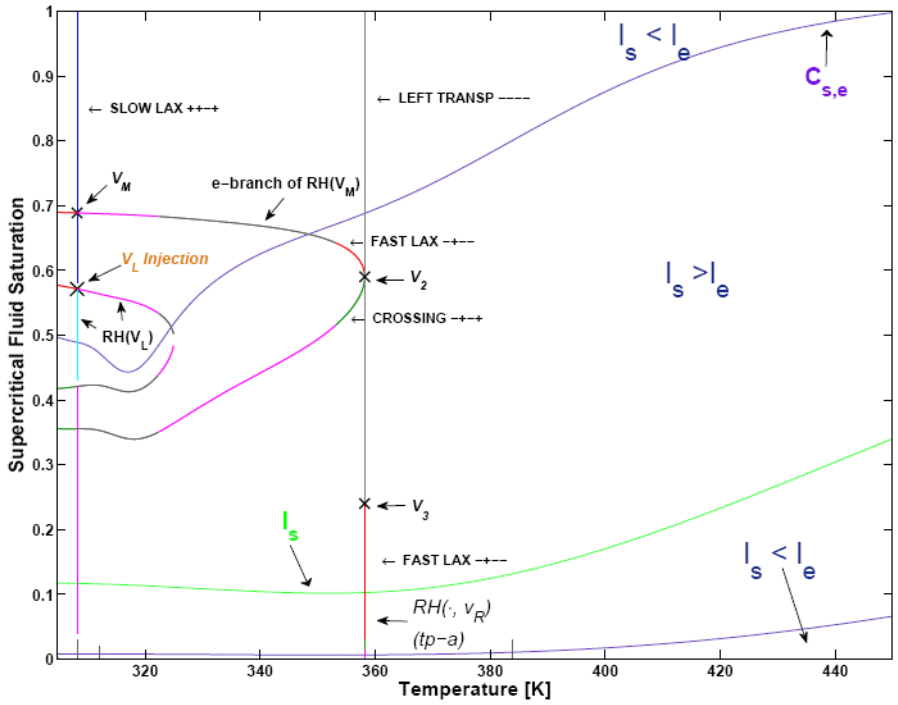

Fig. 6 Wave curves used for finding the Riemann solution. We use the BL-branch (vertical) of the RH Locus passing through V_L, the e-branch of the RH Locus passing through V_M, the BL-rarefaction curve through V_2, and the *tp-a* RH Locus with right state V_R.

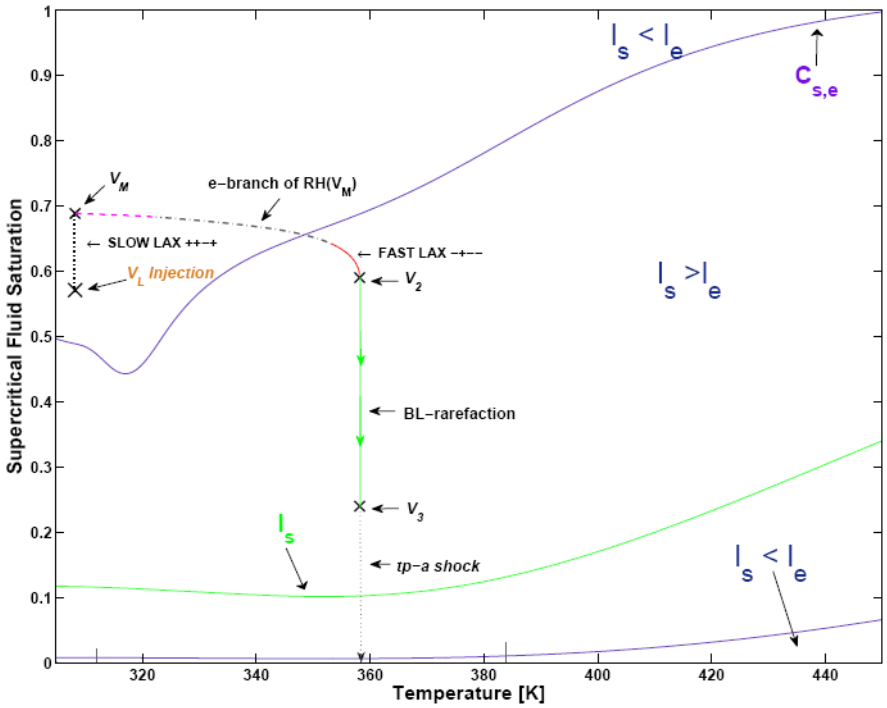

Fig. 7 The wave sequence for the CO_2-EGS example. There exists a slow Lax BL shock wave between V_I and the intermediate state V_M, and a fast Lax *e*-shock wave between V_M and V_2. The speed of the latter is equal to the derivative of the fractional flow function calculated on V_2. A BL rarefaction wave connects V_2 and V_3. Finally there exists *tp-a* shock wave between V_3 and the right state V_R (see Fig. 5), travelling with speed equal to the derivative of the fractional flow function calculated on V_3.

In Figs. 8-12 we present the profile of the solution for the injection problem at a fixed positive time. For the numerical values of the quantities defined in these figures, see the appendix section. The slowest wave is a Buckley-Leverett saturation shock. At the time of this snapshot, this shock is located at P_1. Upstream of P_1 there is a region containing the injected CO_2/H_2O mixture. As it can be seen in the remaining figures, only the saturation varies throughout this shock. There is a slightly faster evaporation/condensation shock, which is located at P_2, where we observe an abrupt change in saturation and temperature (changes of the latter account for the change in the compositions of CO_2 and H_2O in the supercritical and aqueous phase, respectively) as well as a shock in the seepage speed. Downstream of this shock there is a Buckley-Leverett rarefaction wave up to P_3, along which saturation varies. At P_3 there is a shock wave separating a two-phase mixture upstream, from pure water downstream. All quantities vary along this shock, which is the fastest wave. Downstream of this shock there is a region containing the pure hot water initially present in the reservoir.

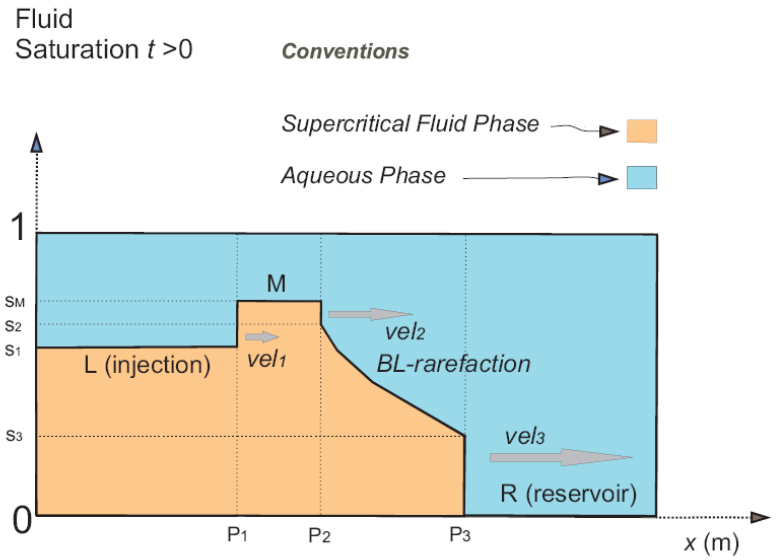

Fig. 8 Saturation profile. Arrows size indicates relative speed.

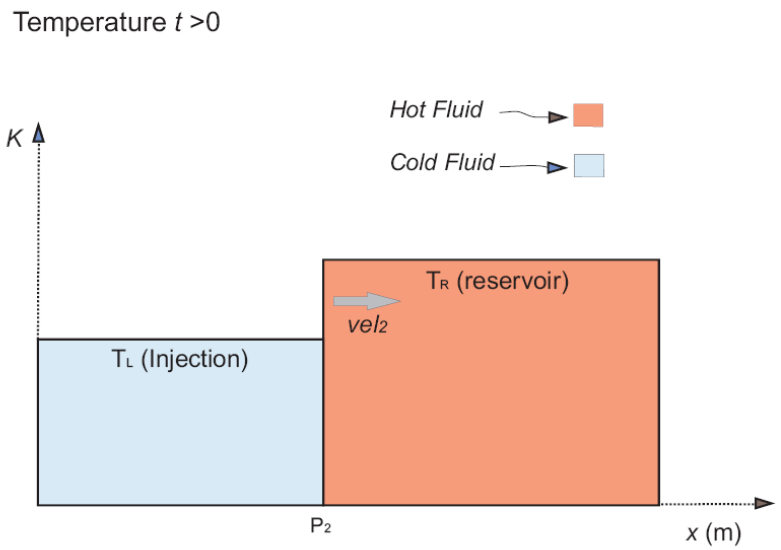

Fig. 9 Temperature profile.

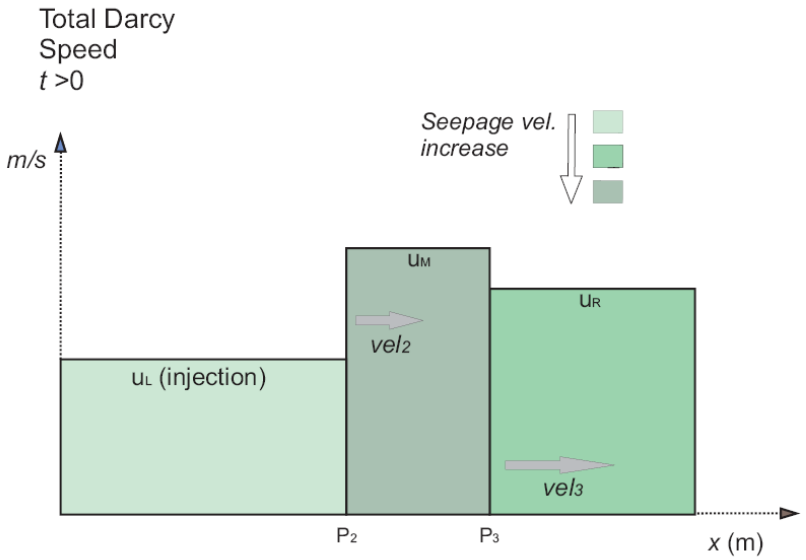

Fig. 10 Seepage speed.

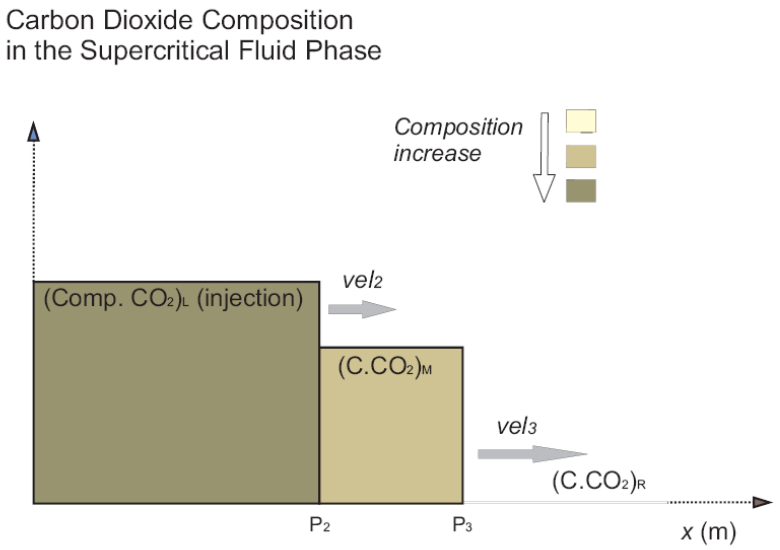

Fig. 11 Carbon Dioxide composition profile.

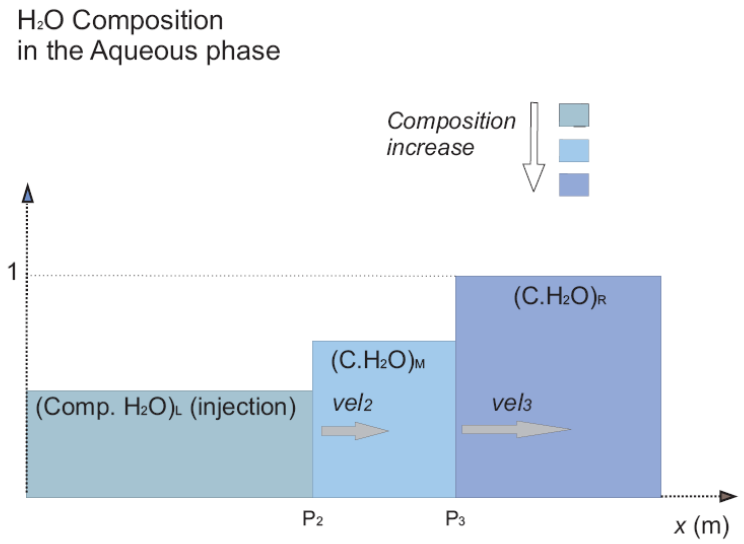

Fig. 12 Water composition profile.

Conclusions

- Simultaneous injection of cold carbon dioxide and water in a geothermal reservoir combines the advantage of geothermal energy recovery and sequestration of CO_2.
- Using the Peng-Robinson equation in combination with activity based mixing rules including a volume shift operation makes it possible to derive equilibrium properties like densities for carbon dioxide/ water mixtures at supercritical conditions.
- Application of the method of characteristics makes it possible to describe the rarefaction waves and shocks that occur for cold CO_2/water injection in a porous medium filled with hot water. The results can be conveniently summarized in a phase diagram for rarefaction waves and a Rankine-Hugoniot (RH) diagram to describe the shocks.
- The wave structure provides a fundamental understanding of non-isothermal flow of mixtures with mass transfer between phases assuming local thermodynamic equilibrium
- At the temperature shock the carbon dioxide concentration in the gas phase decreases due to evaporation of water. The concentration of carbon dioxide in the aqueous phase also decreases downstream of the temperature shock.
- For an injection mixture of carbon dioxide and water the saturation profiles show a complex combination of rarefactions ands shock waves. The temperature wave moves much slower than the carbon dioxide BL wave.
- The phase diagram and RH diagram can de used to construct the solutions in terms of rarefactions, constant states and shock waves. The shock waves must satisfy the entropy conditions; we have verified that Lax and Liu E-condition are satisfied.
- The solution for the Riemann problem is constructed by a sequence of waves that appear between and inside regions of local thermodynamic equilibrium. In a more general setting, the structure of the solution may depend strongly on the injection and initial reservoir conditions. Some of the configurations of the solutions are favorable and others are not favorable for practical goals.
- This study provides a fundamental understanding of the non-isothermal flow of mixtures undergoing mass transfer between phases. Analytical solutions for CCS process can be used as powerful tools for studying the mechanisms of sub-surface transport, can provide a simple methodology to screen injection conditions for maximal storage of carbon dioxide, can be applied to validate complex numerical simulators, , and may be particularly useful replacing these simulators for geological times, as the accumulation of numerical errors may be intolerable.

Acknowledgments

We thank Professor Frederico Furtado, and Professor Vitor Matos for their valuable comments on Bifurcation Locus for Riemann Problems.

The hospitality of the Section of Geo-engineering at Delft University of Technology, and the Instituto de Matemática Pura e Aplicada, is gratefully acknowledged.

References

Azevedo, A., De Souza, A., Furtado, F., Marchesin, D. Plohr, B. *The Solution by the Wave Curve Method of Three-Phase Flow in Virgin Reservoirs*, Transport in Porous Media, Published Online June 2009.

Bamberger, A., G. Sieder and G. Maurer (2000). "*High-pressure (vapor+ liquid) equilibrium in binary mixtures of (carbon dioxide+ water or acetic acid) at temperatures from 313 to 353 K.*" The Journal of Supercritical Fluids **17**(2): 97-110.

Buckley, S. E. and M. C. Leverett (1942). "*Mechanism of fluid displacement in sands.*" Trans. AIME **146**: 107-116.

Dafermos, C. *Hyperbolic Conservation Laws in Continuum Physics*, Third Edition, Springer, Heidelberg, 2010.

Dahl, S. and M. Michelsen (1990). "*High-pressure vapor-liquid equilibrium with a UNIFAC-based equation of state.*" AIChE journal **36**(12): 1829-1836.

Gmelin Institute for Inorganic Chemistry of the Max-Planck-Society for the Advancement of Science, Founded by L.Gmelin. *Handbook of Inorganic and Organometallic Chemistry*, Springer-Verlag 8th Edition.

Hebach, A., A. Oberhof and N. Dahmen (2004). "*Density of water+ carbon dioxide at elevated pressures: measurements and correlation.*" J. Chem. Eng. Data **49**(4): 950-953.

Huang, H. and S. Sandler (1993). "*Prediction of vapor-liquid equilibria at high pressures using activity coefficient parameters obtained from low-pressure data: a comparison of two equation of state mixing rules.*" Industrial & Engineering Chemistry Research **32**(7): 1498-1503.

Huron, M. and J. Vidal (1979). "*New mixing rules in simple equations of state for representing vapour-liquid equilibria of strongly non-ideal mixtures* 1.*" Fluid Phase Equilibria **3**(4): 255-271.

Isaacson, E., Marchesin, D., Plohr, B. *Transitional Waves for Conservation Laws*, Siam J. Math. Anal. Vol. 21, No.4, pp. 837-866, July 1990.

Isaacson, E., Marchesin, D., Plohr, B., Temple, J.B. *Multiphase flow models with singular Riemann problems*, Mat. Apl. Comput. 11 (2) 147-166 (1992).

King, M., A. Mubarak, J. Kim and T. Bott (1992). "*The mutual solubilities of water with supercritical and liquid carbon dioxides* 1.*" The Journal of Supercritical Fluids **5**(4): 296-302.

Kongsjorden, H., O. Kårstad and T. Torp (1998). "*Saline aquifer storage of carbon dioxide in the Sleipner project.*" Waste management **17**(5-6): 303-308.

Koschel, D., J. Coxam, L. Rodier and V. Majer (2006). "*Enthalpy and solubility data of CO2 in water and NaCl (aq) at conditions of interest for geological sequestration.*" Fluid Phase Equilibria **247**(1-2): 107-120.

Lambert, W. Marchesin, D., *The Riemann problem for compositional flows in porous media with mass transfer between phases,* Journal of Hyperbolic Differential Equations, Vol 6, No.4 p. 725-751, (2009).

Lambert, W., Marchesin, D. And Bruining, J., The Riemann Problem for the injection of steam and nitrogen in a porous medium, IMPA, Transport in Porous Media, Published online June 9 (2009).

Lauwerier, H. (1955). "*The transport of heat in an oil layer caused by the injection of hot fluid.*" Applied Scientific Research **5**(2): 145-150.

Leveque, R.J. *Finite Volume Methods for Hyperbolic Problems* Cambridge Texts in Applied Mathematics, (2002).

Orbey, H. and S. Sandler (1998). *Modeling vapor-liquid equilibria: cubic equations of state and their mixing rules*, Cambridge Univ Pr.

Péneloux, A. and E. Rauzy Richard (1982). "*A consistent correction for Redlich-Kwong-Soave volumes.*" Fluid Phase Equilibria **8**(1): 7-23.

Peng, D. and D. Robinson (1976). "*A new two-constant equation of state.*" Industrial & Engineering Chemistry Fundamentals **15**(1): 59-64.

Pritchett, J. W. (2009). *On the relative effectiveness of H_2O and CO_2 as reservoir working fluids for EGS heat mining*. Transactions - Geothermal Resources Council. **33:** 211-216.

Pruess, K. (2008). "*On production behavior of enhanced geothermal systems with CO2 as working fluid.*" Energy Conversion and Management **49**(6): 1446-1454.

R. Farajzadeh, P. R., P. L.J. Zitha, and J. Bruining (2010). *The Effect of Heterogeneity on the Character of Density-Driven Natural Convection of CO2 Overlying a Brine Layer*, Canadian Society for Unconventional Gas, Calgary, Society of Petroleum Engineers, SUG/**SPE 123399**

Reinsch, C., *Smoothing by Spline Functions*, Numerische Mathematik 10, pp. 177-183, (1967).

Renon, H. and J. Prausnitz (1968). "*Local compositions in thermodynamic excess functions for liquid mixtures.*" AIChE journal **14**(1): 135-144.

Renon, H. and J. Prausnitz (1969). "*Estimation of parameters for the NRTL equation for excess Gibbs energies of strongly nonideal liquid mixtures.*" Industrial & Engineering Chemistry Process Design and Development **8**(3): 413-419.

Riddiford, F., I. Wright, C. Bishop, T. Espie and A. Tourqui (2004). *Monitoring geological storage: the in Salah gas CO2 Storage Project*.

Salimi, H., Bruining, H., *Upscaling in Vertically Fractured Oil Reservoirs Using Homogenization.* Transport in Porous Media, Published online 22 Oct. 2009

Sandarusi J.A. Yesavage V.F., *Compilation of parameters for a polar fluid Soave-Redlich-Kwong equation of state*. *Ind. Eng. Chem. Process Des. Dev.*, 25 (4) (1986), pp. 957-963.

Span R., and Wagner W., *A new equation of state for carbon dioxide covering the fluid region from the triple-point temperature to 1100 K at pressures up to 800 MPa, J. Phys. Chem. Ref. Data 25*, (6) (1996), pp. 1509-1596.

Smöller, J., Shock Waves and Reaction-Diffusion Equations, Springer-Verlag, (1983).

Smith, J., H. Van Ness and M. Abbott (2001). *Introduction to chemical engineering thermodynamics*, McGraw-Hill.

Stryjek, R. and J. Vera (1986). "*PRSV: An improved Peng-Robinson equation of state for pure compounds and mixtures.*" The canadian journal of chemical engineering **64**(2): 323-333.

Valtz, A., A. Chapoy, C. Coquelet, P. Paricaud and D. Richon (2004). "*Vapour-liquid equilibria in the carbon dioxide-water system, measurement and modelling from 278.2 to 318.2 K.*" Fluid Phase Equilibria **226**: 333-344.

Walas, S. (1985). *Phase equilibria in chemical engineering*, Butterworth Boston.

Wendland M., Hasse H., And Maurer G. *Experimental pressure temperature data on three and four phase equilibria of fluid, hydrate, and ice phases in the system carbon dioxide-water, J. Chem. Eng. Data 44, 5, pp. 901-906 (1999)*

Wiebe, R. and V. Gaddy (1939). "*The solubility in water of carbon dioxide at 50, 75 and 100, at pressures to 700 atmospheres.*" Journal of the American Chemical Society **61**(2): 315-318.

Zuluaga, E. and L. Lake (2005). *Semianalytical Model for Water Vaporization in Gas Producers*. SPE. **SPE 93862**.

Zuluaga, E. and L. W. Lake (2004). *Modeling of experiments on water vaporization for gas injection*. SPE. **91393:** 15-17.

Zweigel, P., R. Arts, A. LOTHE and E. Lindeberg (2004). "*Reservoir geology of the Utsira Formation at the first industrial-scale underground CO2 storage site (Sleipner area, North Sea).*" Geological storage of carbon dioxide: 165.

Appendix

The numerical values of the quantities in Figs. 8-12 are:

Fig. 8: $s_1 = 0.5713$, $s_2 = 0.5901$, $s_3 = 0.24$, $s_M = 0.689$, $vel_1 = 0.1158\ [m/s]$, $vel_2 = 0.3039\ [m/s]$, $vel_3 = 2.2937\ [m/s]$.

Fig. 9: $T_L = 308.15\ [K]$, $T_R = 358.15\ [K]$.

Fig. 10: $u_L = 4.22 \times 10^{-6}\ [m^3/m^2 \cdot s]$, $u_M = 10.94 \times 10^{-6}\ [m^3/m^2 \cdot s]$, $u_R = 9.28 \times 10^{-6}\ [m^3/m^2 \cdot s]$.

Fig. 11: $(\text{Comp. } CO_2)_L = \frac{662\ [kg/m^3]}{665\ [kg/m^3]}$, $(\text{Comp. } CO_2)_M = \frac{216.81\ [kg/m^3]}{218.23\ [kg/m^3]}$, $(\text{Comp. } CO_2)_L = 0$.

Fig. 12: $(\text{Comp. } H_2O)_L = \frac{943.63\ [kg/m^3]}{998.2\ [kg/m^3]}$, $(\text{Comp. } H_2O)_L = \frac{952.63\ [kg/m^3]}{998.2\ [kg/m^3]}$, $(\text{Comp. } H_2O)_L = 1$.